

Parabolic Hall Effect in Weyl Metals

M. Breitzkreuz*

Dahlem Center for Complex Quantum Systems and Fachbereich Physik,
Freie Universität Berlin, 14195 Berlin, Germany

(Dated: November 2019)

A real-space separation of countermoving states to opposite surfaces is realized in various condensed-matter systems, leading to different types of Hall effects, such as the quantum-, spin- or the anomalous-Hall effect. Weyl metals with intrinsically or extrinsically broken inversion and time-reversal symmetries provide the possibility to separate a fraction of countermovers in a completely different fashion: Forward movers homogeneously distributed in the bulk and back movers localized at the surfaces. In this work we show that this special type of chiral separation is associated with a novel Hall effect — a parabolic transverse potential profile induced by current along the magnetic field. The Hall voltage of this parabolic Hall effect is measurable in the geometry of a hollow cylinder between the inner and the outer surfaces and via associated characteristic effects in the longitudinal resistivity.

Introduction—The condensed-matter realization of Weyl fermions [1–7] has attracted very much interest in the past years, due in large part to the novel transport phenomena [8, 9]. Many of them are related to the probably most peculiar property of Weyl fermions that the lowest Landau level is chiral, moving parallel or antiparallel to the magnetic field, depending on the Weyl-fermion chirality [10]. In a crystal, the two chiralities appear pairwise, separated in momentum space and in energy but not in real space so that a net chiral current can only be produced if the two chiralities are brought out of balance. Unfortunately, a non-equilibrium situation like this activates also other transport channels, hence it is typically hard to isolate Weyl-specific transport phenomena such as the chiral magnetic effect [11–14].

Tentatively it is more promising when chiral states are separated not (or not only) in momentum but in real space, a situation well known from the separation of countermovers to opposite surfaces in topological insulators [15] signified, e.g., by quantum (spin) Hall effects [16, 17]. A noteworthy pendant in the field of Weyl metals is the anomalous Hall effect (AHE) [18, 19] — a voltage drop in the direction perpendicular to both, the direction of the current flow and the intrinsic magnetization, in the absence of an external magnetic field. The strength of the AHE is commonly quantified by the Hall angle, which is the ratio of the Hall electric field and the field along the current flow; currently Weyl metals hold the record with values of around 20% [20–22].

The mechanism of the AHE in Weyl metals can indeed be understood in terms of spatially separated chiral states: A pairwise connection of Weyl Fermi surfaces of opposite chirality by two Fermi arcs [23], localized at opposite surfaces and moving in opposite directions, which intuitively explains the Hall conductivity as the contribution of Fermi arcs in case of a potential difference between the surfaces [8, 24], see Fig. 1. In this finite-size view, the bulk Weyl fermions themselves only contribute to the longitudinal conductivity and can be considered as con-

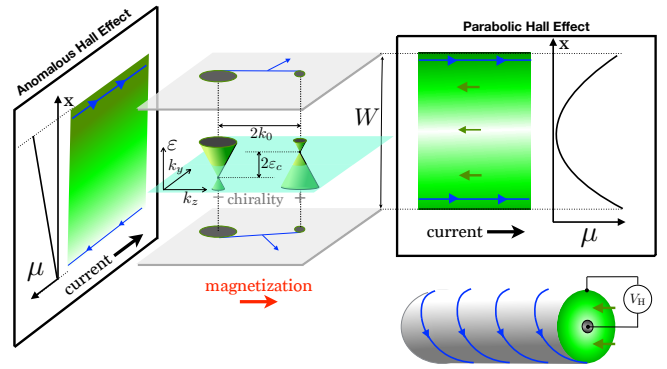


FIG. 1. Weyl-metal slab with two Weyl cones separated in energy and in momentum, connected by Fermi arcs at the surfaces, illustrated in a mixed momentum/real space. Anomalous Hall effect occurs if current is led perpendicular to the magnetization direction and leads to a linear drop of the chemical potential μ between the surfaces. The parabolic Hall effect occurs when current is led parallel to the magnetization, leading to a quadratic spatial dependence of the chemical potential, measurable in the geometry of a hollow cylinder between the inner and outer surfaces.

ventional, diffusive charge carriers. For later reference we note that this implies that the chemical potential μ varies linearly in the bulk because the current density of diffusive bulk particles is proportional to the gradient of the chemical potential, $j_n \propto \nabla\mu$, which combined with particle conservation, $\nabla \cdot j_n = 0$, gives $\Delta\mu = 0$.

In this work we show that in Weyl metals there is in fact another possibility for a spatial separation of chiral states — forward movers homogeneously distributed in the bulk and back movers localized at the surfaces — leading to a novel Hall response, characterized by a *quadratic* (instead of linear) spatial dependence of μ in response to a current led *parallel* (instead of perpendicular) to the magnetization or the magnetic field. The bulk-surface separation of chiral states requires external or intrinsically broken inversion and time-reversal

symmetries. We here consider a minimal model, where both symmetries are broken intrinsically, consisting of two Weyl nodes lying at different energies as shown in Fig. 1. In this case, both Fermi arcs acquire an equilibrium current density component in the direction of the magnetization, which is the direction of cone separation, while the chiral counter-movers live at the Weyl cones and are delocalized in the bulk producing a homogeneous equilibrium current density j_c . An electric field E aligned with the magnetization then pumps charge between the surface and the bulk, balanced by the diffusive bulk current. Combining both statements, we have $E \propto \nabla \cdot j_c = -\nabla \cdot j_n$, which is equivalent (since $j_n \propto \nabla \mu$) to $\Delta \mu = \text{const.} \neq 0$, hence a quadratic dependence of the potential on the spatial coordinates — an effect that we call the parabolic Hall effect (PHE). In the following we present a detailed calculation of the PHE and its signatures.

Model—Measuring energy in units of $\hbar v$, where v is the Fermi velocity, and length in units of the lattice constant, the Hamiltonian we consider reads

$$H = -\sigma_x i \partial_x + k_y \sigma_y + m(k_z) \sigma_z + \varepsilon_c \eta(k_z), \quad (1)$$

where σ_i are Pauli matrices, $m(k_z) = (k_z^2 - k_0^2)/2k_0$, and $\eta(k_z) = \tanh(2k_z/k_0)$, featuring two Weyl nodes with chirality \pm at momentum $k_{x,y} = 0$, $k_z = \pm k_0$ and energy $\varepsilon \approx \pm \varepsilon_c$. We focus on the case of two well-separated Weyl cones with vanishing corrections to the linear dispersion and a constant velocity v at the Fermi level ε_F , hence $\varepsilon_c, |\varepsilon_F| \ll k_0$. The explicit form of $m(k_z)$ and $\eta(k_z)$ is unimportant as long as these requirements are fulfilled.

Considering a slab of width W the quantum numbers are k_y, k_z , and q , the latter being the solution of

$$\frac{m(k_z)}{q} \tan(Wq) + 1 = 0 \quad (2)$$

coming from the boundary condition of the slab [25]. Throughout this work we assume $W \gg 1$, in which case

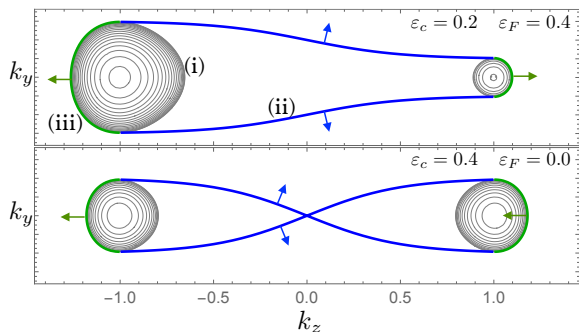


FIG. 2. Fermi-level states for the Weyl metal of width $W = 100$, $k_0 = 1$, and two different combinations of ε_F and ε_c s. The gray, blue, and green states correspond to (i) normal bulk state, (ii) surface states, and (iii) chiral bulk states, respectively. Velocity directions are indicated by arrows.

the solution for q can be divided into three groups, (i) the group of bulk states, given by the quasi continuous set $q = (n + 0.5)\pi/W$, $n = 0, 1, 2, \dots$, (ii) surface states with the imaginary (and hence exponentially decaying) solution $q = i m(k_z)$ for $m(k_z) < 0$, and (iii) chiral bulk states with the solution $q = 0$ for $m(k_z) > 0$. The dispersion reads

$$\varepsilon_k = \varepsilon_c \eta(k_z) \pm \sqrt{q^2 + k_y^2 + [m(k_z)]^2} \quad (3)$$

and the equi-energy contours are illustrated in Fig. 2. Note that surface states (ii) and chiral bulk states (iii) merge at $m(k_z) = 0$ building a single closed contour.

Since the x dependence of the wavefunctions is given by $\exp(i q x)$, the finite penetration depth of surface states is given by $1/\text{Im } q$. The free spectral function in the center-of-mass coordinate $r = (x, y, z)$ and the $W \gg 1$ limit can be written as

$$A(k, r, \omega) = \delta(\omega - \varepsilon_k) \rho(k, x), \quad (4)$$

$$\rho(k, x) = \begin{cases} 1 & \text{Im } q = 0 \\ 2W m(k_z) e^{\pm 2m(k_z)(x \mp W/2)} & \text{Im } q \neq 0 \end{cases} \quad (5)$$

where $\text{Im } q = 0$ and $\text{Im } q \neq 0$ distinguishes bulk and surface states, and \pm corresponds to surface states at $x = \pm W/2$. Despite the divergence of penetration at $m(k_z) = 0$, the surface-state spectral weight averaged over all states at the surface is strongly localized, the characteristic length scale being $1/k_0 \sim 1$. Since all other length scales will be considered to be much larger, we approximate the $\text{Im } q \neq 0$ case in (5) as $\rho(k, x) \approx W \delta(x \mp W/2)$ in the following.

The density of bulk states at the Fermi level of the cone \pm and the total bulk density $n_n = \sum_{\pm} n_{\pm}$, read, respectively,

$$n_{\pm} = \frac{(\varepsilon_F \mp \varepsilon_c)^2}{\pi v \hbar}, \quad n_n = \frac{\varepsilon_F^2 + \varepsilon_c^2}{\pi v \hbar}. \quad (6)$$

In accord with $W \gg 1$, we assume that n_n is much larger than $n_{c\pm}$ and n_s/W , where $n_{c\pm}$ is the density of chiral bulk states and n_s is the 2D density of surface states of a single surface, explicitly reading

$$n_{c\pm} = \frac{|\varepsilon_F \mp \varepsilon_c|}{2v \hbar W}, \quad n_s = \frac{k_0}{\pi v \hbar}. \quad (7)$$

The total particle current in equilibrium is zero in agreement with the general band theory — it is related to the fact the density-of-states weighted integral over the velocity of each closed equi-energy contour is zero and all the contours are closed in a periodic system, see in particular Fig. 2. However, the *local* equilibrium current density is finite in our system because the spatial probability density of states on the special contour containing

surface and chiral bulk states is inhomogeneous. Explicitly, the local equilibrium current density of surface states and chiral bulk states is given, respectively, by

$$j_s^{eq,z}(r) = \frac{1}{W} \int \frac{dk_y dk_z d\omega}{(2\pi)^2} A(k, r, \omega) n_F(\varepsilon_k) v_k$$

$$= \delta(x \pm W/2) \int d\varepsilon \bar{n} v_s^z n_F(\varepsilon), \quad (8)$$

$$j_{c\pm}^{eq,z} = \int d\varepsilon \bar{n} v_{c\pm}^z n_F(\varepsilon), \quad (9)$$

where $n_F(\varepsilon)$ is the equilibrium occupation function and $\bar{n} v_{s/c}^z$ is the density-of-states weighted integral over the velocity at energy ε ; at the Fermi level, we obtain

$$\bar{n} v_{c\pm} = \pm \frac{\varepsilon_F \mp \varepsilon_c}{\pi \hbar W}, \quad \bar{n} v_s^z = \frac{\varepsilon_c}{\pi \hbar} = \frac{\varepsilon_c}{k_0} n_s v. \quad (10)$$

The relation $\bar{n} v_{c+} + \bar{n} v_{c-} = -2\bar{n} v_s^z/W$, signifies the vanishing total current in equilibrium, $\int dx (j_{c+}^{eq,z} + j_{c-}^{eq,z} + j_s^{eq,z}) = 0$.

Parabolic Hall effect—To explore the transport behavior in linear response, we aim to find a solution for a state-dependent deviation of the chemical potential from the Fermi energy, $\mu(k, r)$, with an arbitrary spatial dependence, given the boundary condition of a homogeneous force field in the z direction $\partial_z \mu(k, r) = E$. Furthermore we assume elastic scattering from a weak disorder potential. To focus on qualitative features, we take the scattering amplitudes different only between Fermi-level states of the different types $i \in [n+, c+, s+, n-, c-, s-]$. Using the Quantum Boltzmann formalism [26] and employing the standard semiclassical approximation scheme, see Supplemental Material for details [27], we obtain

$$\nabla \cdot (j_{n\pm} + j_{c\pm}) = \pm \gamma_{n-n+} (\mu_{n-} - \mu_{n+}) + \gamma_{sn\pm} s(x) (\mu_s - \mu_{n\pm}), \quad (11a)$$

$$s(x) \nabla \cdot j_{s\pm} = s(x) [\gamma_{sn+} (\mu_{n+} - \mu_{s\pm}) + \gamma_{sn-} (\mu_{n-} - \mu_{s\pm})], \quad (11b)$$

$$j_{n\pm} = -n_{\pm} D \nabla \mu_{n\pm}, \quad (11c)$$

where $\gamma_{ij} = \Gamma_{ij} n_i n_j$ and Γ_{ij} is the scattering rate, $\mu_i = \langle \mu(k, r) \rangle_i$ is the local chemical potential averaged over the Fermi-level states i , $j_i = n_i \langle v_k \mu(k, r) \rangle_i$ is the non-equilibrium current-density contribution of the states i , D is the bulk diffusion constant, and $s(x) = \sum_{\pm} \delta(x \pm W/2)$.

To linear order in E and using translation invariance in the y direction, the divergence of the chiral-bulk and the surface particle currents simplify to

$$\nabla \cdot j_{c\pm} = \bar{n} v_{c\pm} E, \quad \nabla \cdot j_{s\pm} = \bar{n} v_s^z E, \quad (12)$$

where $\bar{n} v_i$ are given in (10). We rewrite Eqs. (11) by considering the differential Eqs. (11a) away from the boundary ($s(x) = 0$), together with (11c) and (12),

$$\bar{n} v_{c\pm} E - n_{n\pm} D \partial_x^2 \mu_{n\pm} = \pm \gamma_{n+n-} (\mu_{n-} - \mu_{n+}). \quad (13)$$

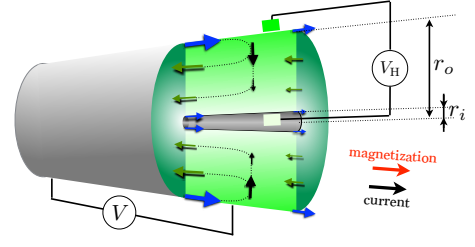


FIG. 3. Weyl metal in the geometry of a cylinder with a small inner radius. When current is led along the cylinder and the magnetization, the PHE voltage is induced between the inner and the outer surface. Arrows indicate local current flows of chiral bulk (green), surface (blue), and diffusive bulk (black) particles.

This is supplemented with boundary conditions, given by integration of (11) over a small distance at both boundaries and assuming vanishing current through the boundary,

$$j_{n+}^x(\pm W/2) = \mp \gamma_{sn+} (\mu_{s\pm} - \mu_{n+}(\pm W/2)), \quad (14a)$$

$$j_{n-}^x(\pm W/2) = \mp \gamma_{sn-} (\mu_{s\pm} - \mu_{n-}(\pm W/2)), \quad (14b)$$

$$E \bar{n} v_s^z = \gamma_{sn+} (\mu_{n+}(\pm W/2) - \mu_{s\pm}) + \gamma_{sn-} (\mu_{n-}(\pm W/2) - \mu_{s\pm}). \quad (14c)$$

Assuming that an external contact would couple to all bulk states with equal probability it would probe the averaged chemical potential

$$\mu_n = \frac{n_{n+} \mu_{n+} + n_{n-} \mu_{n-}}{n_n}, \quad (15)$$

for which Eqs. (13) and (14) readily provide the solution

$$\mu_n = -\frac{n_s v}{n_n D} \frac{\varepsilon_c}{k_0} \frac{x^2}{W} E + z E. \quad (16)$$

Sticking to the interpretation that the $z E$ term stems from the applied voltage, the response lies in the first term in (16), which exhibits the PHE — a quadratic spatial dependence on the transverse coordinate.

Measuring the Hall voltage—As it is evident from Eq. (16), the geometry of the slab does not allow the measurement of the PHE voltage since the potential is the same at both surfaces. To measure the PHE voltage one needs to break this symmetry, which is most conveniently done in the geometry of a hollow cylinder, see Fig. 3, where the two surfaces are bend at different radii, the inner radius r_i and the outer radius r_o .

A straightforward modification of the above formalism [27] [essentially consisting in the replacements $W \rightarrow r_o - r_i$, $x \rightarrow r$, $\partial_x j_n^x \rightarrow (\partial_r + 1/r) j_n^r$] leads to the solution

$$\mu_n = -\frac{n_s v}{n_n D} \frac{\varepsilon_c}{k_0} \left(\frac{r^2/2}{r_o - r_i} - \frac{r_o r_i}{r_o - r_i} \ln \frac{r}{r_i} \right) E + z E, \quad (17)$$

which gives a finite Hall voltage $\mu_n(r_o) - \mu_n(r_i)$ between the outer and the inner surface. Defining the Hall angle for the PHE as $\theta_{\text{PHE}} \equiv [\mu_n(r_o) - \mu_n(r_i)]/(r_o - r_i)E$ in the limit $r_o \gg r_i$, we obtain

$$\theta_{\text{PHE}} = -\frac{n_s v}{n_n D} \frac{\varepsilon_c}{2k_0}. \quad (18)$$

Note that the first factor, $n_s v/n_n D \equiv \theta$, is the Hall angle of the AHE [19, 24], which is thus related to θ_{PHE} by the ratio of energy- vs. momentum separation of the Weyl nodes (energy in units of $\hbar v$).

Resistivity—We now turn to the signatures of the PHE in the behavior of the longitudinal resistivity, given by $\rho = E/(j_n^z + \bar{j}_c^z + \bar{j}_s^z)$, where j_c^z and j_s^z are averaged over x . The non-equilibrium current-density contributions of the surface and the chiral bulk states are given by (8) and (9), with $n_F(\varepsilon)$ replaced by the non-equilibrium part of the occupation, $n'_F(\varepsilon)\mu_i(r)$. Note that we neglected a correction stemming from the state dependence of the potential, which is suppressed by a factor $1/W$. The contribution of normal bulk states is obtained from (11c), it would give the resistivity $\rho_0 = E/j_n^z = -1/n_n D$ if one would neglect the PHE i.e., the quadratic dependence of $\mu_i(r)$. In terms of ρ_0 the actual inverse resistivity reads

$$\frac{\rho_0}{\rho} = 1 + \frac{4}{3}\theta_{\text{PHE}}^2 \left(1 + \frac{6l_{ns}}{W\theta}\right) \left(1 + \frac{\varepsilon_F^2}{\varepsilon_c^2}\xi\right), \quad (19)$$

$$\xi = \frac{\frac{2l_c}{W} - \frac{\left(\frac{2l_c}{W}\right)^2}{\frac{l_{ns}}{\theta l_c} + \coth \frac{W}{2l_c}}}{\frac{W}{6l_c} + \frac{l_{ns}}{\theta l_c}} = \begin{cases} 0 & l_c \ll W \\ 1 & l_c \gg W, l_{ns}/\theta, \end{cases} \quad (20)$$

where $l_{ns} = v/\Gamma_{sn}n_n$ is the relaxation length of surface states and $l_c = \sqrt{D/\Gamma_{n+n}n_n}$ is the internode relaxation length [28]. The correction due to the PHE, proportional to the square of the Hall angle, is similar to the conventional (anomalous) Hall effect, where the correction to the inverse resistivity would be given by $(n_s v/n_n D)^2$, in our model this can be reproduced by leading the current in a direction perpendicular to the magnetization. The finite-size correction in the first brackets is also similar to the finite-size correction of the AHE, recently discussed in [24], and is due to the vanishing dissipation of surface states if their scattering length becomes large compared to the width W . The second brackets correspond to a finite-size correction which occurs if the system is not electron-hole compensated ($\varepsilon_F \neq 0$), in which case the applied field induces an occupation disbalance between the Weyl nodes leading to a prolonged relaxation time. The resistivity decrease saturates even if $l_c \rightarrow \infty$ because internode relaxation also happens indirectly via surface states.

Discussion—Our calculations have shown how a non-linear potential profile can be produced in systems where a small fraction of countermovers are displaced between the bulk and the surface, thus producing uncompensated

chiral states in the bulk. Note that the number of normal (i.e. non-chiral) bulk states is $\sim W$ (in units of the lattice constant) times larger than the number of chiral states but the mean separation of countermovers by $\sim W$ compensates this so that the effect survives the limit $W \rightarrow \infty$. While we have based our calculations on a specific microscopic model of a Weyl metal and Quantum Boltzmann formalism, the general reason for the non-linear potential is based on the simple transferable rule that spatially separated chiral states act as particle sources or drains when a driving field E_{\parallel} is aligned with their motion,

$$\Delta\mu = E_{\parallel}/\lambda, \quad (21)$$

where the characteristic length λ depends on the relative densities and mobilities of the chiral and diffusive particles.

Our model exemplifies such a situation in a Weyl metal with intrinsically broken inversion and time-reversal symmetries, which shows a homogeneous chiral charge density in the bulk, giving $\lambda = W/4\theta_{\text{PHE}}$. Alternatively (or additionally) it is possible to induce (or change) the chiral charge density externally. For example, internode charge pumping via parallel electric and magnetic fields can effectively shift the energies of the Weyl nodes as

$$\varepsilon_c \rightarrow \varepsilon_c + \frac{e^2}{\hbar^2} \frac{\tau}{n_n} EB, \quad (22)$$

where τ is the internode relaxation time [11]. Another interesting possibility to induce and control the PHE is the application of a strain-induced pseudomagnetic field [29–31], which allows to change the separation of chiral states even without an electric field and independent of the internode relaxation.

Furthermore, the derived unconventional dependence of the resistivity on the system size and the scattering amplitudes as a consequence of the PHE, is an interesting starting and reference point for investigations of the resistivity with regard to temperature dependence in case of phonon-mediated scattering [32], or the scaling behaviour with the system size [33]. It is worth noting that in a time-reversal invariant Weyl metal, the mechanism of a reduced and size-dependent resistivity due to a doubling of the AHE [24], also applies to the PHE. The PHE voltage would vanish but the associated suppression of the resistivity would remain when the coupling between the time-reversed states is sufficiently weak. The suppression would set in when the width W becomes comparable to the characteristic scattering length quantifying the coupling of time-reversed states.

Acknowledgments. The author would like to thank Piet W. Brouwer and Tobias Meng for valuable discussions. This research was supported by the Grant No. 18688556 of the Deutsche Forschungsgemeinschaft (DFG, German Research Foundation).

-
- * breitrk@physik.fu-berlin.de
- [1] S.-Y. Xu, N. Alidoust, I. Belopolski, Z. Yuan, G. Bian, T.-R. Chang, H. Zheng, V. N. Strocov, D. S. Sanchez, G. Chang, C. Zhang, D. Mou, Y. Wu, L. Huang, C.-C. Lee, S.-M. Huang, B. Wang, A. Bansil, H.-T. Jeng, T. Neupert, A. Kaminski, H. Lin, S. Jia, and M. Zahid Hasan, *Science* **349**, 613 (2015).
 - [2] S.-Y. Xu, N. Alidoust, I. Belopolski, Z. Yuan, G. Bian, T.-R. Chang, H. Zheng, V. N. Strocov, D. S. Sanchez, G. Chang, C. Zhang, D. Mou, Y. Wu, L. Huang, C.-C. Lee, S.-M. Huang, B. Wang, A. Bansil, H.-T. Jeng, T. Neupert, A. Kaminski, H. Lin, S. Jia, and M. Zahid Hasan, *Nat. Phys.* **11**, 748 (2015).
 - [3] B. Q. Lv, H. M. Weng, B. B. Fu, X. P. Wang, H. Miao, J. Ma, P. Richard, X. C. Huang, L. X. Zhao, G. F. Chen, Z. Fang, X. Dai, T. Qian, and H. Ding, *Phys. Rev. X* **5**, 031013 (2015).
 - [4] S. Borisenko, Q. Gibson, D. Evtushinsky, V. Zabolotnyy, B. Büchner, and R. J. Cava, *Phys. Rev. Lett.* **113**, 027603 (2014).
 - [5] M. Neupane, S.-Y. Xu, R. Sankar, N. Alidoust, G. Bian, C. Liu, I. Belopolski, T.-R. Chang, H.-T. Jeng, H. Lin, A. Bansil, F. Chou, and M. Z. Hasan, *Nat. Commun.* **5**, 3786 (2014).
 - [6] Z. K. Liu, B. Zhou, Y. Zhang, Z. J. Wang, H. M. Weng, D. Prabhakaran, S. K. Mo, Z. X. Shen, Z. Fang, X. Dai, Z. Hussain, and Y. L. Chen, *Science* **343**, 864 (2014).
 - [7] J. Xiong, S. K. Kushwaha, T. Liang, J. W. Krizan, M. Hirschberger, W. Wang, R. J. Cava, and N. P. Ong, *Science* **350**, 413 (2015).
 - [8] N. P. Armitage, E. J. Mele, and A. Vishwanath, *Rev. Mod. Phys.* **90**, 015001 (2018).
 - [9] B. Yan and C. Felser, *Annu. Rev. Condens. Matter Phys.* **8**, 337 (2017).
 - [10] H. B. Nielsen and M. Ninomiya, *Phys. Lett. B* **130(6)**, 389 (1983).
 - [11] A. A. Burkov, *Annu. Rev. Condens. Matter Phys.* **9**, 359 (2018).
 - [12] A. A. Burkov, *Phys. Rev. B* **96**, 041110(R) (2017).
 - [13] S. Nandy, G. Sharma, A. Taraphder, and S. Tewari, *Phys. Rev. Lett* **119**, 176804 (2017).
 - [14] R. D. dos Reis, M. O. Ajeesh, N. Kumar, F. Arnold, C. Shekhar, M. Naumann, M. Schmidt, M. Nicklas, and E. Hassinger, *New J. Phys.* **18**, 085006 (2016).
 - [15] X. L. Qi and S. C. Zhang, *Rev. Mod. Phys.* **83**, 1057 (2011).
 - [16] K. von Klitzing, *Rev. Mod. Phys.* **58**, 519 (1986).
 - [17] M. König, S. Wiedmann, C. Brüne, A. Roth, H. Buhmann, L. W. Molenkamp, X.-L. Qi, and S.-C. Zhang, *Science* **318**, 766 (2007).
 - [18] A. A. Burkov and L. Balents, *Phys. Rev. Lett* **107**, 127205 (2011).
 - [19] A. A. Burkov, *Phys. Rev. Lett* **113**, 187202 (2014).
 - [20] T. Suzuki, R. Chisnell, A. Devarakonda, Y.-T. Liu, W. Feng, D. Xiao, J. W. Lynn, and J. G. Checkelsky, *Nat. Phys.* **12**, 1119 (2016).
 - [21] E. Liu, Y. Sun, L. Müchler, A. Sun, L. Jiao, J. Kroder, V. Süß, H. Borrmann, W. Wang, W. Schnelle, S. Wirth, S. T. B. Goennenwein, and C. Felser, *Nat. Phys.* **14**, 1125 (2018).
 - [22] P. Li, J. Koo, W. Ning, J. Li, L. Miao, L. Min, Y. Zhu, Y. Wang, N. Alem, C.-X. Liu, Z. Mao, and B. Yan, arXiv:1910.10378.
 - [23] L. Balents, *Physics* **4**, 36 (2011).
 - [24] M. Breitkreiz and P. W. Brouwer, *Phys. Rev. Lett* **123**, 066804 (2019).
 - [25] N. Bovenzi, M. Breitkreiz, T. E. O'Brien, J. Tworzydło, and C. W. J. Beenakker, *New J. Phys.* **20**, 023023 (2018).
 - [26] G. D. Mahan, *Many-Particle Physics* (Kluwer Academic, New York, 2000).
 - [27] See Supplemental Material for details of the derivation and solution of transport equations for the slab and the hollow-cylinder geometry.
 - [28] S. A. Parameswaran, T. Grover, D. A. Abanin, D. A. Pesin, and A. Vishwanath, *Phys. Rev. X* **4**, 031035 (2014).
 - [29] D. I. Pikulin, A. Chen, and M. Franz, *Phys. Rev. X* **6**, 041021 (2016).
 - [30] A. G. Grushin, J. W. F. Venderbos, A. Vishwanath, and R. Ilan, *Phys. Rev. X* **6**, 041046 (2016).
 - [31] J. Behrends, S. Roy, M. H. Kolodrubetz, J. H. Bardarson, and A. G. Grushin, *Phys Rev B* **99**, 140201 (2019).
 - [32] R. G. Pereira, F. Buccheri, A. De Martino, and R. Egger, *Phys. Rev. B* **100**, 035106 (2019).
 - [33] C. Zhang, Z. Ni, J. Zhang, X. Yuan, Y. Liu, Y. Zou, Z. Liao, Y. Du, A. Narayan, H. Zhang, T. Gu, X. Zhu, L. Pi, S. Sanvito, X. Han, J. Zou, Y. Shi, X. Wan, S. Y. Savrasov, and F. Xiu, *Nat. Mater.* **18**, 482 (2019).

SUPPLEMENTAL MATERIAL

Quantum Boltzmann formalism

To explore the transport behavior in linear response, but at the same time allowing non-linear dependencies on the spatial coordinate, we use the Quantum Boltzmann Transport formalism allowing an arbitrary spatial variation of the Wigner distribution function $f(k, r, \omega)$ [26]. In this inhomogeneous case, an external field, inducing the steady non-equilibrium state, can be incorporated via non-equilibrium boundary conditions on the spatial variation of the distribution, hence no explicit external field will be needed. Assuming impurity scattering in first Born approximation (T matrix given by impurity-potential matrix elements V_{kp}) and assuming that the associated renormalization of the dispersion relation is already incorporated in ε_k , the kinetic equation reads

$$v_k \cdot \nabla f(k, r, \omega) = A(k, r, \omega) \int \frac{d^3p}{(2\pi)^3} |V_{kp}|^2 f(p, r, \omega) - f(k, r, \omega) \int \frac{d^3p}{(2\pi)^3} |V_{kp}|^2 A(p, r, \omega). \quad (\text{S1})$$

Following the standard route, from the Wigner distribution function $f(k, r, \omega)$ we factor out the spectral density $A(k, r, \omega)$ such that $f(k, r, \omega) = f(k, r)A(k, r, \omega)$, defining the non-equilibrium occupation function $f(k, r)$. Assuming weak scattering, we employ the quasiparticle approximation and use the free-particle expression (4) for the spectral function. Inserting into (S1) and integrating over ω , we obtain the Boltzmann equation

$$v_k \cdot \nabla f(k, r) = \sum_p \Gamma_{kp} [f(p, r) - f(k, r)], \quad (\text{S2})$$

where we divided both sides by $\rho(k, x)$ (keeping in mind that Eq. (S2) becomes trivial if $\rho(k, x) = 0$, i.e., for surface states away from the boundary). In the Boltzmann Equation we defined

$$\sum_p \Gamma_{kp} \dots = \int \frac{d^3p}{(2\pi)^3} |V_{kp}|^2 \delta(\varepsilon_k - \varepsilon_p) \rho(p, x) \dots \quad (\text{S3})$$

To focus more deeply on qualitative features, we assume that the scattering amplitudes are different only between states of the different types, so that $\Gamma_{kp} \rightarrow \Gamma_{ij}$, where $i, j \in [n+, c+, s+, n-, c-, s-]$. In this case, the integral over states naturally splits into integrals over the different particle types,

$$\begin{aligned} \sum_p &= \sum_{p^\pm}^{n^\pm} + \sum_{p^\pm}^{c^\pm} + s(x) \sum_p^s, \\ \sum_p^{n^\pm} &= \int^{n^\pm} \frac{d^2p}{4\pi^2 \hbar v}, \quad \sum_p^{c^\pm} = \frac{1}{W} \int^{c^\pm} \frac{dp}{2\pi \hbar v}, \quad \sum_p^s = \int^{s^\pm} \frac{dp}{2\pi \hbar v}, \end{aligned} \quad (\text{S4})$$

where $s(x) = \sum_\pm \delta(x \pm W/2)$. Since the Boltzmann equation (S2) is non-trivial only for the non-equilibrium part of the occupation, the usual ansatz $f(k, r) = n_F(\varepsilon_k) + n'_F(\varepsilon_k) \mu(k, r)$, where $n_F(\varepsilon_k)$ is the equilibrium occupation function, replaces $f(k, r) \rightarrow \mu(k, r)$ in (S2). We define the non-equilibrium chemical potential and the particle-current density of each particle type i , respectively, as

$$\mu_i = \sum_k^i \mu(k, r) / n_i, \quad j_{i\pm} = \sum_k^i v_k \mu(k, r), \quad (\text{S5})$$

where $n_i = \sum_k^i$ is the density of states of the particle type i . Defining the diffusion constant of bulk particles as $D = v^2/3 \sum_p \Gamma_{n\pm p}$ and summing the Boltzmann equation (S2) over $n\pm$ after multiplying with v_k and assuming the Weyl Fermi surfaces to be spherical, we obtain

$$j_{n\pm} = -n_\pm D \nabla \mu_{n\pm}. \quad (\text{S6})$$

Summing the Boltzmann equation (S2) over each particle type gives

$$\nabla \cdot j_{n\pm} = \pm (\gamma_{c\mp n\pm} + \gamma_{n-n+}) (\mu_{n-} - \mu_{n+}) + \gamma_{sn\pm} s(x) (\mu_s - \mu_{n\pm}), \quad (\text{S7a})$$

$$\nabla \cdot j_{c\pm} = \pm \gamma_{n\mp c\pm} (\mu_{n-} - \mu_{n+}) + \gamma_{sc\pm} s(x) (\mu_s - \mu_{c\pm}), \quad (\text{S7b})$$

$$s(x) \nabla \cdot j_{s\pm} = s(x) [\gamma_{sn+} (\mu_{n+} - \mu_{s\pm}) + \gamma_{sn-} (\mu_{n-} - \mu_{s\pm}) + \gamma_{sc+} (\mu_{c+} - \mu_{s\pm}) + \gamma_{sc-} (\mu_{c-} - \mu_{s\pm})], \quad (\text{S7c})$$

where $\gamma_{ij} = \Gamma_{ij}n_in_j$ and we assumed that intracone scattering is much larger than intercone and bulk-surface scattering so that $\mu_{n\pm} - \mu_{c\pm} \approx 0$ away from the boundary. Taking into account that the number of normal bulk states n_{\pm} strongly dominates since $W \gg 1$ the equations simplify to (11) in the main text.

Solving the transport equations

We now solve for the case of a homogeneous force field applied in the z direction in form of a potential gradient $\partial_z \mu = E$. To linear order in E and using translation invariance in the y direction, the divergence of the chiral and the surface particle currents simplify to

$$\nabla \cdot j_{c\pm} = \bar{n}v_{c\pm}E, \quad \nabla j_{s\pm} = \bar{n}v_s^z E. \quad (\text{S8})$$

A solution for the non-equilibrium potential profile in the x direction is found by first solving for the non-equilibrium potential for the bulk. Away from the boundary ($s(x) = 0$) we obtain from (S7), (11c), and (12)

$$\bar{n}v_{c\pm}E - n_{n\pm}D\partial_x^2\mu_{n\pm} = \pm \frac{n_+n_-}{n_n} \frac{D}{l_c^2} (\mu_{n-} - \mu_{n+}), \quad (\text{S9})$$

where we used $\gamma_{c-n+} + \gamma_{n-n+} + \gamma_{n-c+} \approx n_+n_- \Gamma_{n+n-}$ since $n_{c\pm} \ll n_{\pm}$ and defined the chiral relaxation length $l_c \equiv \sqrt{D/\Gamma_{n+n-}n_n}$. Boundary conditions for $\mu_{n\pm}$ are given by integration of (S7) over an infinitesimal distance at both boundaries and assuming vanishing current through the boundary,

$$j_{n+}^x(\pm W/2) = \mp \gamma_{sn+}(\mu_{s\pm} - \mu_{n+}(\pm W/2)) \quad (\text{S10a})$$

$$j_{n-}^x(\pm W/2) = \mp \gamma_{sn-}(\mu_{s\pm} - \mu_{n-}(\pm W/2)) \quad (\text{S10b})$$

$$E\bar{n}v_s^z = \gamma_{sn+}(\mu_{n+}(\pm W/2) - \mu_{s\pm}) + \gamma_{sn-}(\mu_{n-}(\pm W/2) - \mu_{s\pm}). \quad (\text{S10c})$$

We now introduce the bulk chemical potential μ_n , which is the local chemical potential averaged over all bulk states, and the chiral chemical potential μ_a ,

$$\mu_{n/a} = \frac{n_+\mu_n + \pm n_-\mu_n}{n_n} \Leftrightarrow \mu_{n\pm} = n_n \frac{\mu_n \pm \mu_a}{2n_{\pm}}. \quad (\text{S11})$$

Eqs. (S9) and the boundary conditions (S10) partially decouple into

$$\partial_x^2 \mu_n = -2\theta \frac{\varepsilon_c}{k_0} \quad (\text{S12a})$$

$$\partial \mu_n |_{x=\pm W/2} = \mp \theta \frac{\varepsilon_c}{k_0} \quad (\text{S12b})$$

$$\partial_x^2 \mu_a = \frac{1}{l_c^2} [\mu_a - \gamma \mu_n] + 2\theta \frac{\varepsilon_F}{k_0} \frac{E}{W}, \quad (\text{S12c})$$

$$\partial \mu_a |_{x=\pm W/2} = \mp \left[\theta \frac{\varepsilon_c}{k_0} \gamma \left(1 + \frac{\theta W}{4l_{ns}} \right) E + \frac{\theta}{l_{ns}} \mu_a |_{x=\pm W/2} \right], \quad (\text{S12d})$$

where $\gamma = (n_+ - n_-)/n_n$, $l_{ns} = v/\Gamma_{sn}n_n$ is the scattering length of surface states, and

$$\theta = \frac{n_s v}{n_n D} = \frac{v}{2D} \frac{k_0}{\varepsilon_c^2 + \varepsilon_F^2} \quad (\text{S13})$$

is the Hall angle of the AHE associated with the system of two Weyl nodes [18, 24].

The solution of (S12) together with the solution for μ_s from (S10c) read

$$\mu_n = -\theta \frac{\varepsilon_c}{k_0} \frac{x^2}{W} E + z E, \quad (\text{S14a})$$

$$\mu_a = -\frac{\theta}{k_0} W E \left[2 \left(\frac{l_c}{W} \right)^2 \left(\varepsilon_F + \varepsilon_c \gamma \right) \left(1 - \frac{\cosh \frac{x}{l_c}}{\frac{l_{ns}}{\theta l_c} \sinh \frac{W}{2l_c} + \cosh \frac{W}{2l_c}} \right) + \varepsilon_c \gamma \frac{x^2}{W^2} \right], \quad (\text{S14b})$$

$$\mu_{s\pm} = \mu_n |_{x=W/2} - \frac{\bar{n}v_s^z}{n_s v} l_{ns} E = -\frac{\varepsilon_c}{k_0} \theta \left(\frac{1}{4} + \frac{l_{ns}}{\theta W} \right) W E + z E. \quad (\text{S14c})$$

Current density and resistivity

To obtain the longitudinal resistivity, we calculate the current densities in the z direction from (S5) and (S6). The contribution of normal bulk particles is given by

$$j_n = -n_n D E. \quad (\text{S15})$$

The contribution of chiral bulk particles and surface states can first be written as

$$j_c(x) = \sum_{\pm} \bar{n} v_{c\pm} \mu_{\pm}, \quad (\text{S16})$$

$$j_s(x) = \delta(x \pm W/2) \bar{n} v_s^z \mu_s. \quad (\text{S17})$$

Now using Eq. (S11) and the solutions (S14) we obtain

$$\frac{j_c(x)}{j_n} = -\theta^2 \frac{\varepsilon_c^2}{k_0^2} \left[2 \left(\frac{x}{W} \right)^2 + \left(\frac{2l_c}{W} \right)^2 \frac{\varepsilon_F^2}{\varepsilon_c^2} \left(\frac{\cosh \frac{x}{l_c}}{\frac{l_{ns}}{\theta l_c} \sinh \frac{W}{2l_c} + \cosh \frac{W}{2l_c}} - 1 \right) \right], \quad (\text{S18})$$

$$\frac{j_s(x)}{j_n} = \theta^2 \frac{\varepsilon_c^2}{k_0^2} \left(\frac{1}{4} + \frac{l_{ns}}{\theta W} \right) W \sum_{\pm} \delta(x \pm W/2). \quad (\text{S19})$$

Now the resistivity is given by

$$\rho = \frac{E}{\bar{j}_c + \bar{j}_s + j_n}, \quad \bar{j}_i = \frac{1}{W} \int dx j_i(x). \quad (\text{S20})$$

In the absence of the PHE, i.e., if the potential would be homogeneous in the x direction, the contributions of surface and chiral bulk states would cancel each other. In this case, the current would be carried only via normal bulk states and the resistivity would be given by $\rho_0 = E/j_n = -1/n_n D$. Now taking into account the effect of the PHE, the full inverse resistivity in terms of ρ_0 becomes

$$\frac{\rho_0}{\rho} = 1 + \frac{1}{3} \theta_{\text{PHE}}^2 \left(1 + \frac{6l_{ns}}{W\theta} \right) \left(1 + \frac{\varepsilon_F^2}{\varepsilon_c^2} \xi \right), \quad (\text{S21})$$

$$\xi = \frac{\frac{2l_c}{W} - \frac{\left(\frac{2l_c}{W}\right)^2}{\frac{l_{ns}}{\theta l_c} + \coth \frac{W}{2l_c}}}{\frac{W}{6l_c} + \frac{l_{ns}}{\theta l_c}} = \begin{cases} 0 & l_c \ll W \\ 1 & l_c \gg W, l_{ns}/\theta. \end{cases} \quad (\text{S22})$$

Hollow-cylinder geometry

We now calculate the potential μ_n in the geometry of a hollow cylinder. The derivation of the Boltzmann equation (S2) and summation over states leading to Eqs. (S7) is unmodified. For the calculation of μ_n it is sufficient to consider Eqs. (S6), (S7), and (S8), summed over \pm and the sum of n and c states, which then gives

$$j_n = -n_n D \nabla \mu_n, \quad (\text{S23a})$$

$$\nabla \cdot (j_n + j_c) = -s(r) \nabla j_s, \quad (\text{S23b})$$

$$\nabla \cdot j_c = -2 \frac{\varepsilon_c}{k_0} \frac{n_s v}{r_o - r_i} E, \quad (\text{S23c})$$

$$\nabla \cdot j_s = \frac{\varepsilon_c}{k_0} n_s v E, \quad (\text{S23d})$$

where we used (S8), $n_n \gg n_c$, the cancellation of the total equilibrium current,

$$\pi(r_o^2 - r_i^2) \sum_{\pm} \bar{n} v_{c\pm} + 2\pi(r_o + r_i) \bar{n} v_s^z = 0, \quad (\text{S24})$$

and the not altered result for the 2D density-of-states weighted integral over velocity of surface states

$$\bar{n} v_s^z = \frac{\varepsilon_c}{k_0} n_s v. \quad (\text{S25})$$

In cylinder coordinates the divergence $\nabla \cdot j_n$ becomes $(\partial_r + 1/r)j_n^r$, leading to the differential equation

$$(\partial_r + 1/r)\partial_r \mu_n = -2\theta \frac{\varepsilon_c}{k_0} \frac{E}{r_o - r_i}. \quad (\text{S26})$$

The solution satisfying the boundary conditions given in (S23) reads

$$\mu_n = -\frac{n_s v}{n_n D} \frac{\varepsilon_c}{k_0} \left(\frac{r^2/2}{r_o - r_i} - \frac{r_o r_i}{r_o - r_i} \ln \frac{r}{r_i} \right) E + zE. \quad (\text{S27})$$